11982 *Biochemistry* **2009,** *48,* 11982–11993
DOI: 10.1021/bi901532z

BIOCHEMISTRY
including biophysical chemistry & molecular biology
Article

Characterization of a Key Neutralizing Epitope on Pertussis Toxin Recognized by Monoclonal Antibody 1B7[†]

Jamie N. Sutherland and Jennifer A. Maynard*

Department of Chemical Engineering, University of Texas, Austin, Texas 78712

Received September 2, 2009; Revised Manuscript Received November 3, 2009

ABSTRACT: Despite more than five decades of research and vaccination, infection by *Bordetella pertussis* remains a serious disease with no specific treatments or validated correlates of protective immunity. Of the numerous monoclonal antibodies binding pertussis toxin (PTx) that have been produced and characterized, murine IgG2a monoclonal antibody 1B7 is uniquely neutralizing in all in vitro assays and in vivo murine models of infection. 1B7 binds an epitope on the enzymatically active S1 subunit of PTx (PTx-S1) with some linear elements, but previous work with S1 scanning peptides, phage-displayed peptide libraries, and S1 truncation/deletion variants was unable to more precisely define the epitope. Using computational docking algorithms, alanine scanning mutagenesis, and surface plasmon resonance, we characterize the epitope bound by 1B7 on PTx-S1 in molecular detail and define energetically important interactions between residues at the interface. Six residues on PTx-S1 and six residues on 1B7 were identified that, when altered to alanine, resulted in variants with significantly reduced affinity for the native partner. Using this information, a model of the 1B7−S1 interaction was developed, indicating a predominantly conformational epitope located on the base of S1 near S4. The location of this epitope is consistent with previous data and is shown to be conserved across several naturally occurring strain variants, including PTx-S1A, -B (Tohama-I), -D, and -E (18-323) in addition to the catalytically inactive 9K/129G variant. This highly neutralizing but poorly immunogenic epitope may represent an important target for next-generation vaccine development, identification of immune correlates, and passive immunization strategies for pertussis.

Whooping cough, a respiratory infection caused by the bacteria *Bordetella pertussis*, remains the third major cause of infant mortality, resulting in nearly 50 million cases and 350000 deaths per year worldwide (*1*). In spite of widespread vaccination since the 1950s, outbreaks continue to occur in industrialized countries, with more than 15000 probable or confirmed cases in the United States during 2005 (*2*). To control disease, two cellular and 13 acellular vaccines have been tested for safety and immunogenicity in large clinical trials. The pertussis toxin (PTx)[1] is a major virulence factor, and chemically or genetically detoxified PTx is a major component of all acellular vaccine formulations in combination with up to four additional virulence factors (*3*, *4*). These vaccines are highly effective at preventing the severe manifestations of the disease but do not, in general, prevent bacterial colonization. Vaccine-stimulated immunity declines over time, allowing adults and adolescents to present a reservoir for the pathogen (*5*). As a result, booster vaccines were approved for adults and adolescents in 2005 (*5*), and vaccine research in pertussis remains an active area of investigation.

There is a general consensus that humoral immunity dominates protection against *Bordetella* but controversy about which antigens confer protection and the roles of innate and cellular immunity. Some reports claim a correlation between vaccine-induced anti-PTx IgG levels and subsequent protection against disease (*6*), while other groups observe a stronger correlation with anti-pertactin responses (*7*). Mechanistically, only pertactin-specific antibodies in human immune sera display opsonic activity and induce bacterial phagocytosis by human leukocytes (*7*). However, a monovalent vaccine consisting of only PTx is protective, and passively administered anti-*Bordetella*, anti-PTx polyclonal, and some anti-PTx monoclonal antibodies are able to mitigate many disease symptoms and even reverse disease in mice (*4*, *6*, *8*−*10*). In humans, titers of anti-PTx antibodies rise upon disease onset and are predictive of typical disease (*11*). Administration of human immune sera generated from immunized volunteers shortened disease duration and cough rates in a phase 1 safety trial with hospitalized infants, but a larger phase III trial was unable to confirm or refute the benefit, perhaps because the sera were not sufficiently enriched in antibodies of appropriate specificity (*12*).

PTx is a 105 kDa AB_5 toxin structurally similar to cholera and *Escherichia coli* heat labile enterotoxins. The protein mediates the attachment of bacteria to ciliated epithelial cells and exhibits both ADP-ribosylase and NAD glycohydrolase activities. Although not expressed in the related pathogens *Bordetella bronchiseptica* and *Bordetella parapertussis* due to an inactive promoter, PTx is

[†]Financial support from National Institutes of Health Grant AI066239 (to J.A.M.) and the University of Texas at Austin is acknowledged.

*To whom correspondence should be addressed: MC0400, 1 University Station, University of Texas at Austin, Austin, TX 78712. Phone: (512) 471-9188. Fax: (512) 471-7060. E-mail: maynard@che.utexas.edu.

[1]Abbreviations: CD, circular dichroism; CDR, complementarity-determining region; CHO, Chinese hamster ovary; EC_{50}, 50% effective concentration; ELISA, enzyme-linked immunosorbent assay; hu1B7, humanized scFv version of monoclonal antibody 1B7; K_d, equilibrium dissociation constant; m1B7, murine scFv version of monoclonal antibody 1B7; mAb, monoclonal antibody; PTx, pertussis toxin; PTx-S1, pertussis toxin subunit 1; scFv, single-chain antibody; SPR, surface plasmon resonance.

 Published on Web 11/09/2009

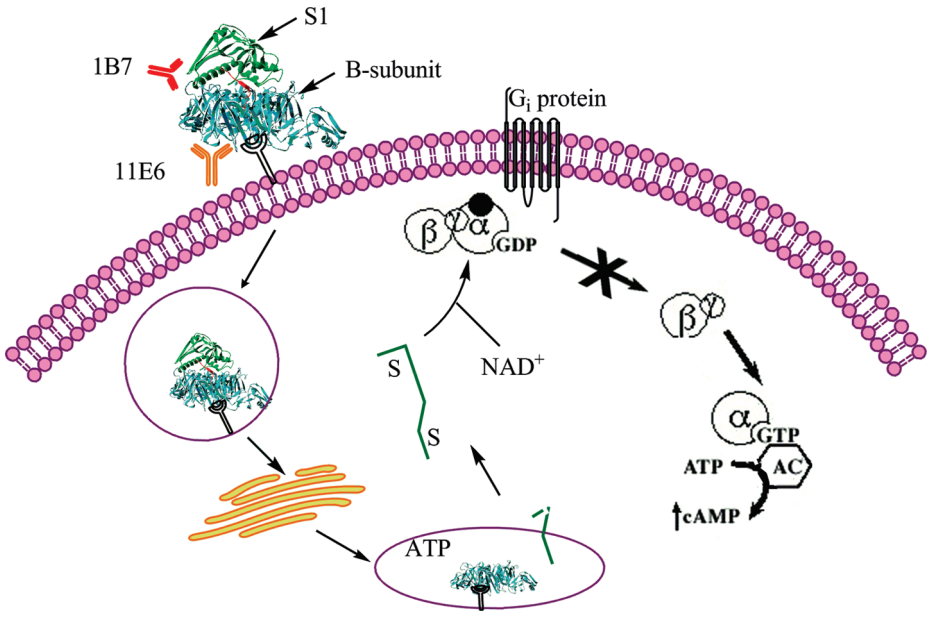

FIGURE 1: Model of pertussis toxin function. The 1B7 antibody neutralizes toxin catalytic function, while the 11E6 antibody competes with the cellular receptor for B oligomer binding. After the toxin binds glycoproteins or glycolipids on the host cell, it undergoes receptor-mediated endocytosis and retrograde transport through the endosome to the Golgi apparatus. From here it is widely believed that PTx is transported to the ER where ATP binds to the central pore of the B oligomer, resulting in the release of the S1 subunit which is subsequently reduced and exposed to the cytosol (it may remain associated with the membrane associated via the hydrophobic tail) (*50*). In the cytosol, PTx-S1 ADP-ribosylates G proteins, disrupting normal signaling and increasing cAMP levels.

required for the long-term persistence of *B. pertussis* (*13*). The B oligomer (S2−S5) of the toxin binds to carbohydrates on many cell types, resulting in endocytosis, and exhibits independent adjuvant effects via ligation of the T cell receptor. Upon internalization, the toxin undergoes retrograde transport to the ER where the catalytically active A (PTx-S1) subunit is translocated to the eukaryotic cytosol. Here, PTx-S1 catalyzes ADP ribosylation of Gα subunits of G_i/G_o signaling complexes (see Figure 1). The disrupted inhibitory signaling cascade leads to transiently high intracellular cAMP levels and general immunosuppression in neutrophils and macrophages (*14*).

In an effort to understand mechanisms of protective immunity in pertussis, large numbers of PTx-specific neutralizing murine monoclonal antibodies have been created and characterized to varying degrees (*15*−*17*). After a panel of 10 antibodies had been screened with a series of in vitro and in vivo assays (ADP ribosylation, leukocyte promotion, islet activation, permeability-increasing activity, CHO cell clustering, hemagglutination, and both aerosol and intracerebral mouse models of infection), monoclonal antibody 1B7 was notably protective in more assays and at lower doses than any other characterized antibody preparation, including polyclonal anti-PTx sera (*8*). 1B7 was able to protect mice when administered up to 7 days after infection, reducing bacterial titers in the lungs as well as PTx concentrations and weakening PTx-related effects. Further studies determined that monoclonal antibody 1B7 acts by binding the PTx-S1 subunit with high affinity ($K_d \sim 5$ nM).

Analysis of monoclonal antibodies binding PTx-S1 has broadly identified a conformational neutralizing epitope near the ADP-ribosyltransferase catalytic center (*18*−*21*). Antibody epitope specificity has been largely inferred from activity assays; for instance, in vitro inhibition of ADP-ribosyltransferase activity but not NAD glycosyltransferase activity was thought to be predictive of protection in the CHO cell clustering assay. This correlation suggested that protective anti-PTx-S1 antibodies act by blocking the PTx-S1 catalytic site (*22*). However, the fine details of molecular recognition are critical, as a screen of anti-PTx antibodies with high in vitro anti-ADP ribosylation activity showed that half did not protect in vivo (*8*). The ability of monoclonal antibody 1B7 to bind PTx-S1 on a Western blot indicates that there is a linear component to this highly conformational epitope. However, experiments using 15-mer peptides covering the entire PTx-S1 sequence were unable to identify any peptide mimicking PTx-S1 binding to protective monoclonal antibodies (*16*). In spite of previous efforts with phage-displayed peptides, toxin truncation, and deletion variants, the precise location of this important epitope remains elusive.

The 1B7 antibody potently neutralizes PTx and is able to independently ameliorate disease in the mouse model. An improved understanding of the mechanism of 1B7-mediated protection as well as the precise epitope bound by 1B7 may be crucial to understanding protective immunity in *Bordetella*. As a first step in describing the epitope, we have developed a model of the 1B7−S1 interaction, based on extensive alanine scanning mutagenesis, a homology model of 1B7, and the crystal structure of PTx (*23*). To facilitate mutagenesis and expression of the binding partners, we reconstructed the 1B7 variable regions as recombinant murine (m1B7) and CDR-grafted human (hu1B7) single-chain antibodies (scAb); similarly, the S1 subunit was truncated to amino acid residues 1−220 to allow periplasmic expression in *E. coli* (*24*). Molecular-level characterization of the neutralizing epitope bound by 1B7 may aid in the development of passive immunotherapies or improved acellular vaccines.

EXPERIMENTAL PROCEDURES

PTx (holotoxin), the full-length PTx-S1 (residues 1−235) protomer, and the B oligomer were purchased from List Biological Laboratories, Inc. (Campbell, CA).

Antibody and Toxin Expression. The S1 subunit was amplified using oligonucleotide primers that truncated PTx-S1

from the amino terminus of the mature, processed protein to carboxy-terminal residue 220, renamed it PTx-S1−220, and subcloned it into expression vector pAK400 (*25*). Expression vector pMoPac16, a pAK400 derivative with a C-terminal human constant κ domain, was used to express scFvs as scAbs, and the residues were numbered using the Kabat numbering system (*26*). Point mutations for both scAbs and the truncated toxin S1 subunit were introduced by around the plasmid PCR (*27*).

Recombinant proteins were expressed in the bacterial periplasm of *E. coli* strain BL21 followed by osmotic shock, and immobilized metal affinity chromatography purification was used to produce and purify all recombinant proteins as previously reported (*28*). Size-exclusion chromatography with PBS as the eluant was used as a polishing step for PTx-S1−220 and m1B7 scAb proteins (Superdex 75 and 200, respectively, GE Healthcare, Uppsala, Sweden). Protein L affinity chromatography was used as a second purification step for the hu1B7 scAb proteins (immobilized Protein L, Pierce, Rockford, IL) using 100 mM Na_2HPO_4 and 150 mM NaCl (pH 7.2) during binding and low-pH IgG elution buffer (Pierce) followed by 1 M Tris (pH 8.0) to neutralize eluted fractions. A micro-bicinchoninic acid assay (Pierce) was used to measure protein concentrations, while SDS−PAGE with GelCode Blue stain reagent (Pierce) was used to verify protein preparation homogeneity and purity.

Antibody−Antigen Binding Analysis. High-binding enzyme-linked immunosorbent assay (ELISA) plates (Costar) were coated with PTx at 1.3 μg/mL or serial dilutions of PTx-S1−220 or its variants and incubated at 4 °C overnight. The plates were then blocked with PBS and 1% milk for 1 h at room temperature. After the sample had been washed three times with PBS and 0.05% Tween 20, anti-PTx antibody (mAb 1B7, m1B7, hu1B7, or hu1B7 variants) was added either in serial dilution or at 8 μg/mL and the mixture allowed to equilibrate at room temperature for 1 h. After three additional washes, peroxidase-conjugated anti-human C_k (Sigma) or peroxidase-conjugated anti-mouse IgG (Sigma) was added for 1 h at room temperature. Finally, the plate was washed three times and developed with tetramethylbenzidine dihydrochloride substrate (Pierce). The reaction was quenched with 1 N HCl and read using a SpectraMax M5 instrument (Molecular Devices) at 405 nm. EC_{50} values were calculated as the concentration at 50% of the maximum response from the linear range of a dose−response curve ($EC_{50} = [A_{405,max} - A_{405,min}]/2$). The percent EC_{50} values were calculated as the ratio of the EC_{50} wild-type reference to the EC_{50} variant ($[EC_{50\text{-WT}}/EC_{50\text{-variant}}] \times 100\%$). Reported percent EC_{50} values are average values, with each experiment being performed at least in triplicate and outliers, defined as values greater than 3 times the median, omitted.

(*i*) *Antibody stability analysis* was performed by incubating duplicate samples of the scAb variant or 1B7 IgG in PBS at 37, 50, and 4 °C for 24, 2, and 24 h, respectively. After incubation, the fraction of active antibody remaining was determined by an ELISA and calculated with reference to an untreated sample maintained at 4 °C.

(*ii*) *CHO cell clustering assays* were performed by incubating 1039 pg/mL PTX with a 100000-fold molar excess of scAb protein for 0.5 h at room temperature in 96-well tissue culture plates. Freshly trypsinized confluent Chinese hamster ovary (CHO) cells were then seeded into the plates at a concentration of 10^5 cells/well. After incubation for 24 h at 37 °C, a microscope was used to examine and score the wells on the basis of clustering morphology on a scale of 0−3 with 0 being no clusters and 3 being all clustered, as described by Hewlett et al. (*29*). Final protective molar ratios were reported as the lowest ratio resulting in no clusters. The working concentration of PTx was determined from a preliminary toxin concentration series that resulted in scoring of 1−3 over the concentration range of 65−1039 pg/mL PTx. To observe this same range with protective scAb activity, we chose the lowest concentration resulting in complete clustering along with a 100000 molar ratio of scAb to PTx based upon CHO cell sensitivity to any free PTx.

(*iii*) *Surface plasmon resonance* (*SPR*) analysis was performed using a BIAcore 3000 instrument (GE Healthcare). CM5 chips (GE Healthcare) that contain carboxymethylated dextran covalently attached to a gold surface were used for all SPR experiments. After activation using a 50/50 solution of 1-ethyl-3-[3-(dimethylamino)propyl]carbodiimide hydrochloride and *N*-hydroxysuccinimide, monoclonal antibody 1B7 was immobilized on the chip surface in 100 mM sodium acetate (pH 5.0) until 750 response units was obtained, at which point the reaction was quenched using 1.0 M ethanolamine-HCl at pH 8.5. Samples of the B oligomer, PTx, PTx-S1, or PTx-S1−220 and variants in HBS buffer (pH 7.4) with 3 mM EDTA and 0.005% Tween at five different concentrations between 50 and 3500 nM were run in duplicate over the chip with a 1 min injection, a 5 min dissociation, and a flow rate of 50 μL/min. A 30 s injection of 2 M magnesium chloride at 30 μL/min was used to regenerate the surface between antibody injections. Baseline correction was calculated by subtracting simultaneous runs over a second flow cell which had been activated and quenched with no protein immobilized on its surface. The off rates were calculated using BIAevaluation (version 3.0) from Pharmacia Biosensor. Because of the low expression levels and varying purity of the PTx-S1−220 variants, the concentration-dependent association and dissociation constants, K_A and K_D, respectively, were not calculated. Instead, off rates, which are typically very sensitive to amino acids changes and do not depend on precise concentration measurements, were compared. Reported values are the average and standard deviation of all off rates calculated for each protein.

(*iv*) *Fluorescence measurements* were performed on a Molecular Devices SpectraMax M5 instrument using 96-well special optics low-fluorescence assay plates (Corning). Measurements were taken on a 200 μL volume of 0.65 μm filtered samples diluted from stock in PBS. Excitation wavelengths of 278 and 295 nm were used for tyrosine and tryptophan, respectively. Emission spectra were recorded every nanometer from 330 to 460 nm. The emission spectrum for PBS was subtracted as background from all sample spectra.

(*v*) *Immunoblotting* (*Western blotting*) was performed using samples electrophoresed on a 12% SDS−PAGE gel followed by transfer to a nitrocellulose filter using standard methods. All toxin samples were loaded at equimolar concentrations except truncated PTx-S1, which was loaded at approximately double the concentration to compensate for impurities and cleavage. After being blocked with 5% PBS-Tween-milk, the membrane was incubated with the mAb 1B7, m1B7, or hu1B7 with scAbs at double the concentration of the monoclonal antibody for 1.5 h. A secondary antibody, either peroxidase-conjugated anti-mouse Fc or anti-human C_k (Sigma), was then added for 1 h with washing both before and after addition. The resulting bound protein bands were visualized using SuperSignal West Dura Extended Duration Substrate (Pierce) coupled with exposure to X-ray film.

(*vi*) *Circular dichroism* spectra from 300 to 190 nm were recorded on a JASCO-815 chiro-optical spectrometer at room temperature.

Table 1: Binding between PTx, Its Subunits, and Naturally Occurring Variants of 1B7

PTx	mutations to wild-type Tohama I (PTx-S1B)	ELISA[a] % $EC_{50\text{-}PTx}$	mAb m1B7 ~750 RU, k_d ($\times 10^{-3}$ s^{-1})
PTx	−	100	0.4 ± 0.6
B oligomer	−	8	2.7 ± 0.6
PTx-S1−235	−	20[b]	1.9 ± 0.3
PTx-S1−220	−	90 ± 10[c]	1.4 ± 0.1
PTx-S1A	M194I	50 ± 40	0.71 ± 0.04
PTx-S1D	D34E, I198V	90 ± 50	0.95 ± 0.05
PTx-S1E	D34E, S162P, I198M	80 ± 30	1.8 ± 0.5
PTx-S1 9K/129G	R9K, E129G	60 ± 30	1.6 ± 0.7

[a]All ELISAs were conducted using hu1B7 as the primary antibody. [b]S1−235 maintained in soluble form in 0.03% CHAPS, 0.1 mM Na_2EDTA, and 10 mM Tris. [c]Because of the low level of expression, only the purest samples were used for these numbers.

A 1 mm path length quartz cell was used to take triplicate readings on 200 μL samples in PBS. A spectrum of PBS was taken and subtracted from each sample spectrum to correct for background. The average of the three spectra for each sample was used for secondary structure analysis using the JASCO software.

Computational Methods. Antibody Modeling Programs. Web Antibody Modeling (*WAM*) (http://antibody.bath.ac.uk/) predicts antibody structure from sequence data by finding template matches for the light and heavy chains separately and then fitting them together using conserved interface residues (*30*). *Rosetta Antibody Beta* (http://antibody.graylab.jhu.edu/) searches the Protein Data Bank (PDB) of crystal structures to find template matches and then utilizes Lennard-Jones potentials, a Lazaridis−Karplus solvation energy model, rotamer internal energies, and H-bonds to predict the antibody structure (*31*). *Z-dock* (http://zdock.bu.edu/) is a fast-Fourier transform-based docking program used to generate initial docked models of the antigen, PTx-S1, and antibody, hu1B7, from separate structural PDB entries (*32*). Once initial experimental data were collected, a predocked model was constructed manually, based on prior experimental data. *RosettaDock* (http://graylab.jhu.edu:8088/) was then used to refine the model by optimizing side-chain and rigid-body orientation using a Monte Carlo coupled with an energy function to return 10 different models (*33*). All probable docked models were submitted for further analysis using Rosetta computational alanine point mutagenesis (http://robetta.bakerlab.org/), which replaces each residue with an alanine and computes the resulting interface energies (*34*, *35*). This results in identification of energetically important residues at the protein−protein interface for each docked model. *Pepsurf* (http://pepitope.tau.ac.il/index.html) is a computational program that predicts both linear and conformational epitopes based upon the crystal structure of the antigen and experimentally determined peptide sequences (*36*). Six peptide sequences determined via phage screening of mAb 1B7 by the Cortese lab (*37*) were used in conjunction with the crystal structure of PTx (*23*) to predict the three "best clusters" on the toxin surface most likely to contain the desired epitope.

RESULTS

Functional Characterization of Truncated PTx-S1, the B Oligomer, and Naturally Occurring PTx-S1 Variants. To facilitate mutagenesis of the toxin, PTx-S1 from strain Tohama I (variant B) was expressed recombinantly in *E. coli*. Yields of full-length PTx-S1 (amino acids residues 1−235) were extremely low due to the presence of a long hydrophobic tail anchoring PTx-S1 into the B oligomer, but a truncated version consisting of amino acid residues 1−220 was expressed and purified from the bacterial periplasm (*24*). Protein purity was assessed by size-exclusion chromatography and SDS−PAGE. Binding between 1B7 and the commercially available holotoxin, PTx-S1(1−235), B oligomer, and recombinant PTx-S1−220 was assessed by ELISA and SPR using a BIAcore 3000 biosensor. PTx-S1 and PTx-S1−220 bound 1B7 with similar kinetics (k_d values of 1.9 and 1.4×10^{-3} s^{-1}, respectively) (see Table 1 and Figure 2). These data indicate that the PTx-S1 truncation does not affect the affinity of 1B7 for PTx-S1, and therefore, the truncated PTx-S1 format was used to generate and analyze all subsequent site-directed toxin variants.

A systematic loss of affinity was observed for both the truncated PTx-S1−220 and full-length PTx-S1 (off rates of 1.4 and 1.9×10^{-3} s^{-1}, respectively) versus the holotoxin (off rate of 0.4×10^{-3} s^{-1}). To explain this loss, we first noticed weak binding between hu1B7 and the B oligomer via ELISA ($EC_{50\text{-}PTx}$ = 8%). More detailed analysis with SPR detected an off rate of 2.7×10^{-3} s^{-1} between the purified B oligomer and immobilized mAb 1B7 when a high concentration of B oligomer was used (1150−2890 nM). When the ELISA was repeated using mAb 1B7, an $EC_{50\text{-}PTx}$ of 30% for B oligomer versus holotoxin was measured.

To address the potential for natural or vaccine-induced epitope drift to result in S1 variants no longer bound by 1B7, we cloned and expressed truncated PTx-S1 proteins (amino acids 1−220) corresponding to three remaining naturally occurring variants (PTx-S1A, PTx-S1D, and PTx-S1E) using site-directed mutagenesis of PTx-S1B. This was also performed for the catalytically inactive, genetically detoxified variant (PTx-S1 9K/129G) which is promoted for use in acellular vaccines to reduce side effects while retaining most adjuvant and protective qualities (*38*). The *B. bronchiseptica* PTx-S1 subunit containing four mutations (D34E, I198T, S209P, and Y161P) was also constructed but did not express sufficiently well enough to include in the analysis (*39*). Reducing and nonreducing SDS−PAGE gels confirmed the correct molecular weight and purity of the naturally occurring PTx-S1−220 variants compared with the parent PTx-S1B from the Tohama I strain. Binding analysis of these S1 variants using ELISA and SPR measured mAb 1B7 off rates for both PTx-S1E and PTx-S1 9K/129G within error of those measured for PTx-S1−220 (1.8 and 1.6×10^{-3} s^{-1}, respectively). Slightly slower off rates were measured for PTx-S1A and -D [0.7 and 0.95×10^{-3} s^{-1}, respectively (see Table 1)]. Thus, the neutralizing epitope recognized by 1B7 is conserved across all known PTx-S1 variants, including laboratory-generated, catalytically inactive variants.

Functional Characterization of 1B7 Recombinant Antibodies. Two recombinant versions of mAb 1B7, murine (m1B7) and humanized (hu1B7) single-chain Fv antibodies (scAb, a scFv with a C-terminal human κ constant domain), were constructed by RT-PCR, overlap PCR, and CDR grafting as previously described (data not shown) (*25*−*27*). This single-gene, single-protein format facilitated rapid site-directed mutagenesis and expression of the resulting variant proteins. To characterize m1B7 and hu1B7 binding behavior, a Western blot containing the B oligomer, PTx, PTx-S1, and PTx-S1−220 in triplicate was probed with mAb 1B7, m1B7, and hu1B7 (see Figure 3). All three

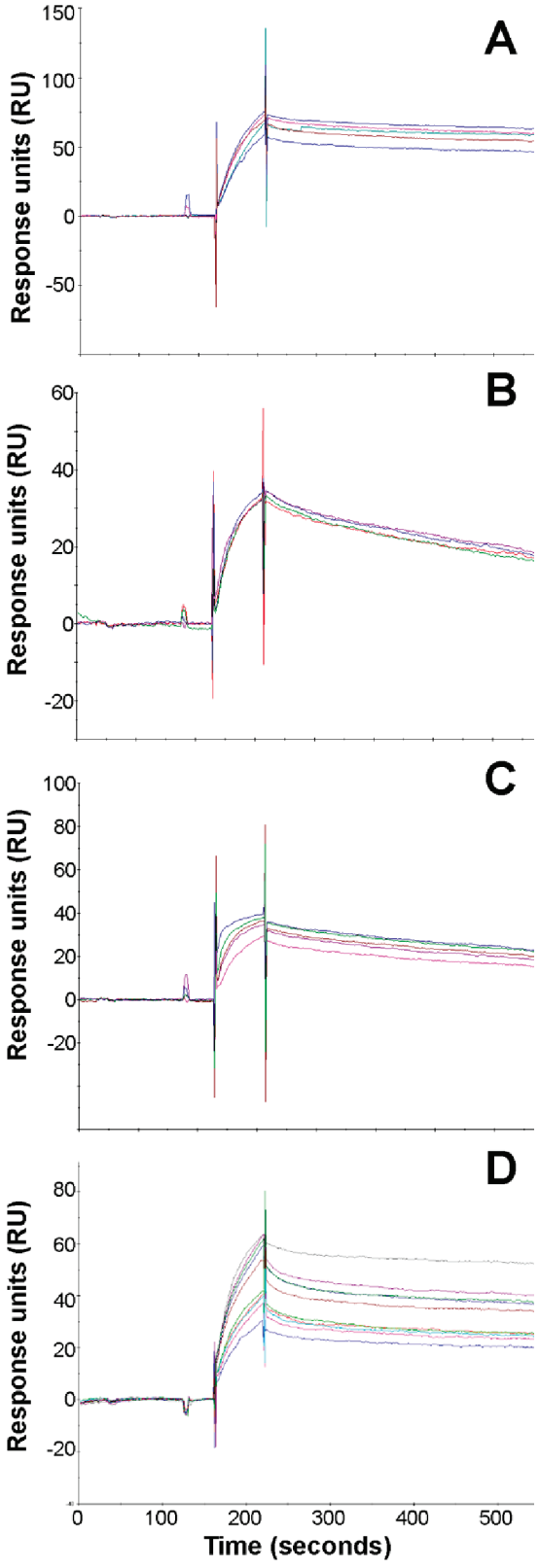

FIGURE 2: Representative BIAcore 3000 (GE Healthcare) SPR runs on a CM5 chip with mAb 1B7 coupled at ~750 RU. (A) PTx holotoxin at 300, 200, 150, 100, and 50 nM. (B) PTx-S1 at 200, 150, 100, and 50 nM. (C) PTx-S1−220 at 300, 200, 150, 100, and 50 nM. (D) B oligomer at 2890, 2300, 2000, 1730, and 1150 nM.

constructs bound PTx-S1 from the holotoxin, PTx-S1, and the truncated PTx-S1−220 with no detectable binding to any of the four remaining subunits. The intensity of the bands corresponds with the affinity of the antibody format for holotoxin or PTx-S1

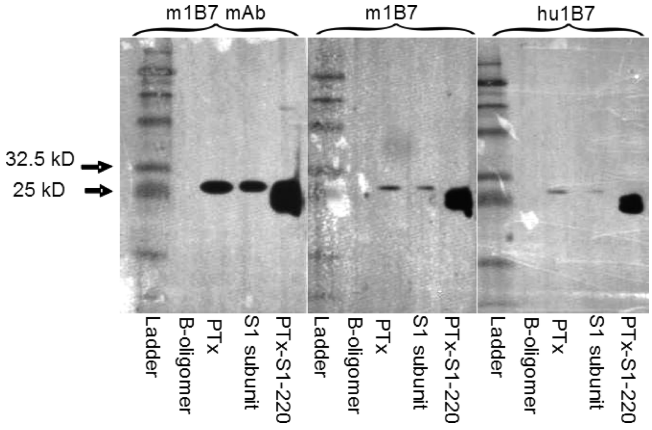

FIGURE 3: Immunoblot analysis of 1B7 antibody constructs. After electrophoresis of 23 pmol of the B oligomer, PTx, and PTx-S1 and 46 pmol of PTx-S1−220 in three identical sections on a 12% SDS−PAGE gel, proteins were electrophoretically transferred to nitrocellulose paper. The antibody constructs mAb 1B7 at 2.9 mg, m1B7 at 5.9 mg, and hu1B7 and 5.9 mg were used to probe a section each with subsequent detection using equivalent amounts of anti-mouse Fc HRP, anti-human C_k HRP, and anti-human C_k HRP, respectively.

Table 2: Binding and Neutralizing Activity of 1B7 Variants

	heat studies $EC_{50\text{-}4°C}$		
antibody	37 °C, 24 h	50 °C, 2 h	CHO cell neutralization assay (μg)
mAb 1B7	100	20	0.09
M1B7	100	40	3
Hu1B7	70	10	9

(mAb 1B7 > m1B7 > hu1B7). Although hu1B7 exhibits the lowest overall binding affinity, this version expressed much better than m1B7 and was used as the parent for site-directed mutagenesis.

A CHO cell neutralization assay was conducted for evaluation of the ability of the antibody constructs to effectively neutralize PTx in an in vitro assay. A prerequisite for success in this assay is thermal stability, as antibodies must retain their binding ability for at least 24 h in serum at 37 °C. To rule out the possibility that hu1B7 scAb variants may not protect in the in vitro assay due to poor thermal stability, antibody samples at 37 μg/mL were heated at 37 °C for 24 h and 50 °C for 2 h prior to binding analysis. The fraction of functional scAb remaining was quantified by ELISA with reference to mock-treated samples. All three constructs (mAb 1B7, m1B7, and hu1B7) retained at least 70% affinity under assay conditions and less than 40% affinity after exposure to the higher temperature (see Table 2). The molar ratio of antibody to toxin required to protect CHO cells in vitro corresponded to the relative antibody binding affinities, with m1B7 requiring a 10-fold and hu1B7 a 30-fold increase in the molar excess of antibody versus mAb 1B7. Despite a drop in affinity relative to the mAb 1B7, both m1B7 and hu1B7 retained the ability not only to bind purified PTx with high affinity but also to effectively neutralize the toxin in vitro.

Computational and Experimental Selection of Residues for Interaction Analysis. To reduce the experimental workload, residues were selected for alanine point mutagenesis analysis in conjunction with two computational methods, (1) ZDock (*32*) coupled with Rosetta Computational Mutagenesis Alanine Scanning (*33*−*35*) and (2) Pepsurf (*36*) coupled with

Table 3: In Silico and Experimental Characterization of hu1B7 and Its Variants

		alanine scan highest		CD spectroscopy[a]			heat studies, $EC_{50\text{-}4°C}$		
antibody	CDR	$\Delta\Delta G_{(complex)}$ (kcal/mol)	$\Delta G_{(partner)}$ (kcal/mol)	% α	% β	ELISA $\%EC_{50\text{-}hu1B7}$	37 °C for 24 h	50 °C for 2 h	CHO cell neutralization assay (μg)
					Binding				
hu1B7	−	−	−	34	38	100	70	10	9
S30A	L1	2.9	0.6	33	49	100 ± 0	100	2	9
N53A	L2	1.2	0.4	23	37	390 ± 30	70	30	9
S92A	L3	1.2	0.3	31	68	50 ± 10	100	5	9
S93A	L3	2.8	1.5	34	28	80 ± 60	100	20	9
S31A	H1	0.2	−0.2	25	19	70 ± 20	100	5	9
F52A	H2	2	2.9	31	44	120 ± 50	70	9	9
					Weakened Binding				
F31A	L1	1.8	2.4	28	28	2 ± 3	60	< 1	NP[b]
H94A	L3	3.1	0.8	27	45	3 ± 4	90	< 1	NP[b]
S97A	H3	2.5	−0.2	29	19	5 ± 4	100	30	NP[b]
					Nonbinding				
W91A	L3	2	3.6	27	44	< 1	−	−	NP[b]
W33A	H1	2	3.5	54	32	< 1	80	< 1	NP[b]
N58A	H2	4.2	0.5	32	23	< 1	90	< 1	NP[b]

[a]These secondary structure values are typical for scFv-huCκ in our hands. [b]No protection.

previously determined 1B7 phage peptides (*37*). Due to the absence of a crystal structure of either hu1B7 or m1B7, two antibody structure prediction algorithms, Rosetta Antibody Beta (*31*) and Web Antibody Modeling (WAM) (*30*), were used to predict four possible antibody structures. All the resulting models had random mean square deviations (rmsd) of approximately 1 Å for the overall structure, the CDR loops, and a few key residues (L-W91A and H-W33A) except the Rosetta hu1B7 model. Due to the similarity of the other three models in addition to the improved expression levels of hu1B7, the hu1B7 WAM model was chosen for subsequent docking models. The crystal structure of PTx-S1 (*23*) and a WAM antibody-predicted structure of hu1B7 were run using method 1, resulting in the prediction of an initial docked model. This was then used for in silico alanine point mutagenesis to guide experiments by predicting which residues would result in the greatest loss of free energy ($\Delta\Delta G$ complex ≥ 1.0 kcal/mol) for each partner. Twelve residues on hu1B7 (see Table 3) and 14 residues on PTx-S1 (see Table 4) were chosen on the basis of their resulting $\Delta\Delta G$ complex, amino acid residues over-represented in protein−protein interactions, and spatial proximity to the binding partner.

Method 2 was performed to take advantage of previously identified peptides mimicking the PTx-S1 epitope. Pepsurf compared the peptide sequences to the holotoxin crystal structure, identifying three potential conformational epitopes on PTx. Only two of these predicted epitopes were likely candidates since the third predicted no binding of PTx-S1. The "best cluster" consisted of the following: A74, G78, R79, G80, T81, H83, and I152 on PTx-S1 and A40 on PTx-S4. Two of these predicted residues, T81 and H83, were also predicted using the first method. If the prediction of partial binding to PTx-S4 is correct, it would explain the reduction in off rates and affinity seen in PTx-S1 versus PTx binding. This weak interaction could be below the sensitivity of either Western blot analysis or SPR or simply nonexistent when looking at PTx-S4 alone due to its sole stabilizing role in the 1B7−PTx-S1 interaction. Unfortunately, we do not have an established expression system for production of PTx-S4 variants and are unable to directly test this interaction. The "second cluster" consisted of the following: P3, P4, A5, P175, N176, and P177 on PTx-S1. This second cluster is highly unlikely since previous studies have determined that the first six residues of PTx-S1 are not involved in the binding of mAb 1B7 (*19*). Amino acid residue N176 was chosen to confirm this hypothesis. Further analysis using the peptide sequences as linear epitopes and comparison with the PTx-S1 amino acid sequence resulted in identification of one additional cluster containing R39. Overall, three additional residues were chosen on the basis of this second method, resulting in a total of 17 PTx-S1 residues for experimental alanine scanning analysis.

Experimental and Computational Residue Analysis. After point mutagenesis to alanine of each chosen residue, each resulting variant was expressed in *E. coli* and purified on at least three separate occasions. These purified variants were first analyzed for a change in affinity toward PTx or WT hu1B7 via ELISA. Variants were categorized as either nonbinding or weakened binding on the basis of average EC_{50} cutoffs of less than 1% or less than 40%, respectively. For WT hu1B7, three variants were determined to be nonbinding (L-W91A, H-W33A, and H-N58A) and three were determined to be weaker binding (L-F31A, L-H94A, and H-S97A). PTx-S1 had four nonbinding variants (R79A, H83A, Y148A, and N150A) and six weaker binding variants (E16A, R39A, T81A, T153A, T158A, and Y166A).

To verify these results, a second assay was performed on each of the variant types. For the hu1B7 variants, heat studies and in vitro CHO cell neutralization assays were performed. The heat studies resulted in all variants retaining >70% affinity under assay conditions, except L-F31A which retained only 60% affinity. The results of the CHO cell assay showed that L-W91A, H-W33A, H-N58A, L-H94A, H-S97A, and L-F31A offer no protection in vitro, thereby confirming the ELISA results. SPR analysis confirmed that PTx-S1 variants R79A,

Table 4: In Silico and Experimental Characterization of PTx-S1−220 and Variants

	alanine scan average		CD spectroscopy			
PTx	$\Delta\Delta G_{(complex)}$ (kcal/mol)	$\Delta G_{(partner)}$ (kcal/mol)	% α	% β	ELISA $\%EC_{50\text{-}PTx}$	mAb m1B7 ~750 RU, k_d ($\times 10^{-3}$ s^{-1})
			Binding			
PTx-S1−220	−	−	11	40	90 ± 10	1.4 ± 0.1
R146A	10.9	3.8	12	42	60 ± 40	1.5 ± 0.1
E155A	0.4	0.6	8	44.1	50 ± 40	1.1 ± 0.1
T156A	0.5	2.5	12	41.6	70 ± 30	1.1 ± 0.1
T159A	3.7	2.1	6	49.8	90 ± 30	1.4 ± 0.2
Y161A	6.5	2.3	11	41.1	50 ± 20	1.3 ± 0.6
N176	0.6	−0.4	13	54	50 ± 20	1.1 ± 0.1
E210A	2.2	0.4	17	33.7	70 ± 40	1.6 ± 0.2
E16A	2.9	−0.3	9	44	20 ± 10	1.6 ± 0.1
T81A	2.8	1.1	9	58	30 ± 10	1.7 ± 0.9
T158A	1.5	1.2	10	42.8	30 ± 20	1.3 ± 0.2
Y166A	4.9	6.8	29	27.2	30 ± 10	1.4 ± 0.2
			Weakened Binding			
R39A	1.1	−0.3	15	43	30 ± 10	3.0 ± 0.4
T153A	1.2	1.0	14	39.2	11 ± 5	2.0 ± 0.4
			Nonbinding			
R79A	0.8	0.1	9	61	1 ± 1	25 ± 4
H83A	3.3	1.4	12	41	< 1	10 ± 2
Y148A	6.6	4.7	9	42	< 1	29 ± 6
N150A	2.1	2.2	6	46	< 1	8 ± 1

H83A, Y148A, and N150A have significantly reduced affinity for mAb 1B7 as seen by their rapid off rates of 25, 10, 29, and 8 × 10^{-3} s^{-1}, respectively. Of the previously classified weaker binding variants, R39A and T153A showed higher off rates than WT PTx-S1−220 (3.0 and 2.0 × 10^{-3} s^{-1}, respectively), while the other four variants, E16A, T81A, T158A, and Y166A, had similar off rates of 1.6, 1.7, 1.3, and 1.4 × 10^{-3} s^{-1}, respectively, thereby changing their classification to binding. The computational methods used to guide experimental efforts correctly predicted residues with experimental $\Delta\Delta G_{(complex)}$ values of >1 kcal/mol with approximately 50% accuracy. The experimental results confirm the most likely cluster predicted with Pepsurf as PTx-S1 residues R79A and H83A were nonbinding in all assays.

Although several variants of both WT hu1B7 and PTx-S1 were identified as nonbinding or weakened binding, this change could be due to indirect structural effects as opposed to a reduction in binding energy. Focusing first on WT hu1B7, we consider three of the identified residues (L-W91, H-W33, and L-H94) structurally relevant in the CDR regions of antibodies (*40*, *41*). The in silico alanine scanning results were then reanalyzed focusing on the value of the calculated $\Delta G_{(partner)}$, for which a value of greater than 1.0 indicates the residue may play a role in stabilizing protein secondary and tertiary structure. This analysis identified residues L-W91, H-W33, and L-F31 as playing structural roles. The final method for determining each residue's contribution to proper folding was experimental comparison of CD analysis of each variant with WT hu1B7. This indicated that experimentally only H-S97A and H-W33A were structurally different from the WT. On the basis of these three methods, only H-W33 consistently appears to be structurally important. However, this residue has ~15% solvent accessibility and has been shown to form hydrogen and π bonds with residues across the interface of the HEL−FabD44.1 interaction (*40*). A similar method was used to determine the structural importance of the PTx-S1 residues. $\Delta G_{(partner)}$ analysis identified all residues except R79 as structural, while CD analysis with comparison to WT PTx-S1−220 indicated only N150A and R79 as being structurally different. Because the results are method-dependent, only N150 can definitely be classified as a structurally important residue. This conclusion is further cemented by structural analysis of PTx-S1 which shows N150 as 7% solvent accessible and playing a key role in a β-sheet structure with five hydrogen bonds with neighboring PTx-S1 residues. Despite the structural roles of both H-W33 on WT hu1B7 and N150 on PTx-S1, the docked model indicates hydrogen bonding of these residues with partner residues across the interface. The model indicates these residues serve dual roles maintaining structural conformation and mediating antigen−antibody binding.

As a final check of whether the identified tryptophan residues (L-W91 and H-W33) are located at the complex interface, tryptophan fluorescence measurements were collected individually for the two tryptophan deficient variants, L-W91A and H-W33A, in addition to WT hu1B7 and PTx-S1−220 (see Figure 4A). Comparison of WT hu1B7 with L-W91A and H-W33A shows relative peaks of 60 and 70%, respectively, indicative of the decrease in the total number of tryptophan residues. While L-W91A shows no shift in peak position, a red shift of 3 nm was observed for H-W33A, signifying tryptophan exposure. This shift is most likely due to a conformational change, which is expected due to the structural role played by this residue. Fluorescence measurements of WT hu1B7, PTx-S1−220, and the equimolar complex of the two were then collected (see Figure 4B). Comparison of the complex with WT hu1B7 and PTx-S1−220 resulted in

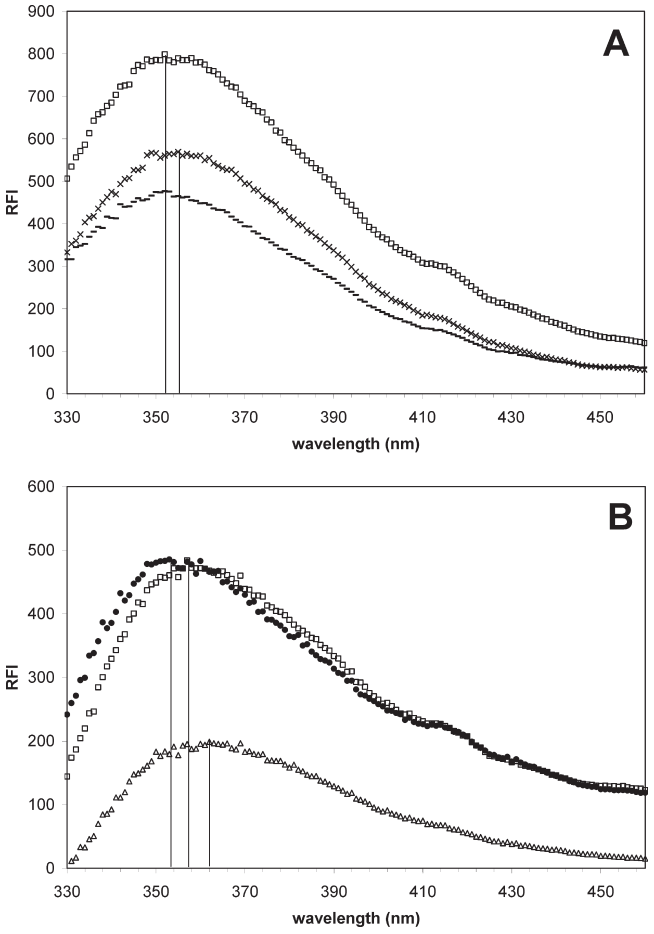

FIGURE 4: Tryptophan fluorescence spectra of hu1B7 (□), L-W91A (—), H-W33A (×), PTx-S1−220 (△), and the hu1B7−PTx-S1−220 complex (◆) in PBS. (A) Comparison of hu1B7, L-W91A, and H-W33A at 4.5 μM and room temperature. Lines indicate spectral peaks at 352, 352, and 355 nm, respectively. (B) Comparison of hu1B7, PTx-S1−220, and the hu1B7−PTx-S1−220 complex at a 1:1 molar ratio at 4.5 μM and room temperature. Lines indicate spectral peaks at 357, 362, and 353 nm, respectively.

blue shifts of 4 and 9 nm, respectively. This masking of the tryptophans (*42*) confirms their presence in the binding interface between WT hu1B7 and PTx-S1−220.

Development and Prediction of the Best Fit Model of Interaction. With these 12 "key binding residues" in mind, as well as the requirements for geometric and electrostatic complementarity to allow binding, WT hu1B7 was manually docked onto PTx-S1 using the molecular viewing programs Swiss PDB Viewer and Pymol to provide a starting complex for computational refinement. The resulting complex was submitted for computational docking using RosettaDock, which is able manipulate the two docked partners ±3 Å toward or away from each other, 8 Å along each other's surface, 8 Å of tilt, and 360° around the center axis between the two (*33*). Of the resulting models, the one which best fit the experimental data, predicting interactions of five of the six PTx-S1 residues and also five of the six WT hu1B7 residues, was selected (see Figure 5). The model predicts hydrogen bonding between N150 and the backbone oxygen of L-W91, H-N58 and the backbone oxygen of H83, N150 and the backbone oxygen of L-S92, and T153 and the backbone oxygen of L-S92. It also predicts hydrogen bonding between several residues determined to be unimportant for binding: E16, R146, L-S92, and L-S93. Although Y148 does not form any predicted hydrogen bonds, it has a large solvation energy effect of 0.14 kcal/mol, indicating solvent interaction. In an examination of the residue side chains, nearly half are aromatic residues with two tryptophans, two histidines, and one tyrosine. Since aromatic clusters are common at protein−protein binding interfaces, comprising ~30% of energetically important residues (*41*), the binding chemistry may involve π bonding or stacking between the two tryptophans on the antibody and the histidine on PTx-S1. Changes in either salt or pH conditions did not significantly affect binding (data not shown), consistent with a binding interface dominated by hydrophobic interactions.

As a final check on the probability of the proposed model, the change in Gibbs free energy for the 1B7−PTx-S1 complex was calculated from experimental equilibrium affinity using the

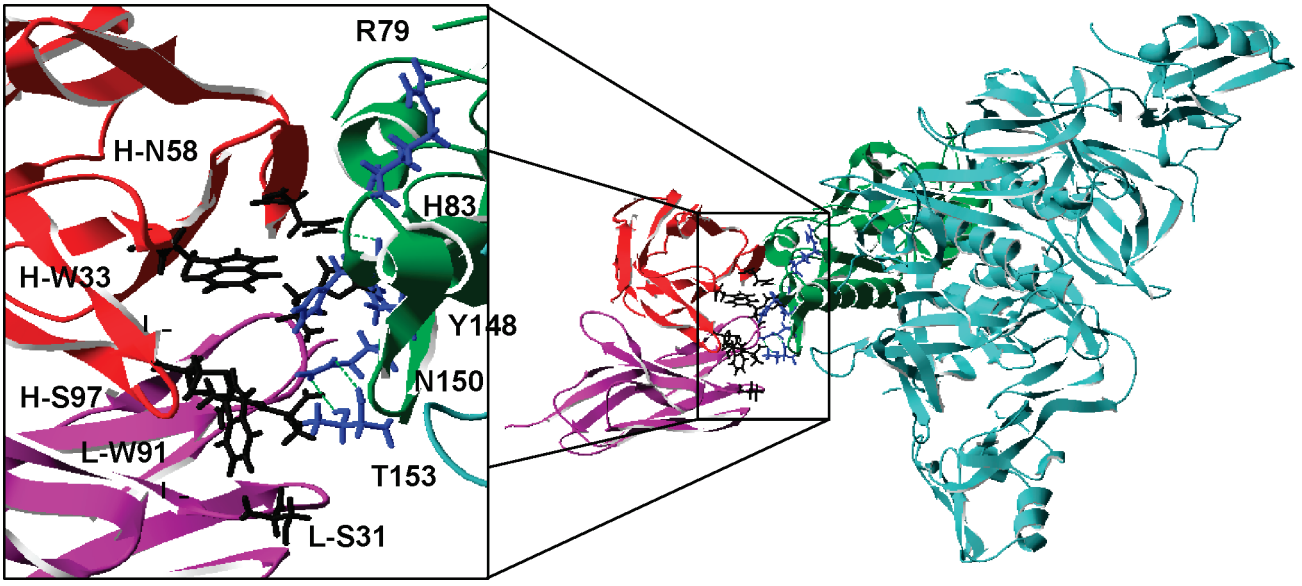

FIGURE 5: 1B7−PTx best fit interaction model generated by RosettaDock using the crystal structure of PTx and the WAM-predicted structure of hu1B7. S1 is colored green, the B oligomer teal, the heavy chain red, and the light chain purple. Experimentally determined important interacting residues on both PTx-S1 and hu1B7 are shown. Colored black are interacting residues on hu1B7 and blue are interacting residues on PTx-S1.

change in Gibbs free energy equation as follows (eq 1):

$$\Delta G = -RT \ln(K_{eq}) = \sum_{i=1}^{n} \Delta\Delta G_i \quad (1)$$

Using the known K_d of 5 nM, the gas constant (R) of 1.987 cal/mol, and 277 K for temperature (T), the ΔG of the complex was calculated to be 10.5 kcal/mol. In the absence of nonadditive cooperative effects (*43*), this value should also equal the sum of the $\Delta\Delta G$ for each binding residue of the complex, with any deviation between these values indicating one or more binding residues have been omitted. In silico computational alanine scanning of the hu1B7−PTx-S1 complex results in a $(\Delta\Delta G)_{sum}$ of 10.5 kcal/mol, very similar to the predicted ΔG and in the predicted range for antibody−antigen complexes (ΔG = 10.9−12.3 kcal/mol for K_d values from 10 to 1 nM). This correspondence indicates that a majority of interacting residues have likely been identified.

DISCUSSION

As the *B. pertussis* organism has not been detected in the blood of patients, it has been suggested that the systemic manifestations are due to toxin release and dissemination. Pittman famously hypothesized that symptoms are mediated primarily by pertussis toxin (PTx), a theory which, 30 years later, remains to be proven. It is clear that PTx is a major antigen, as transposon-insertion mutants of *B. pertussis* manifest greatly reduced virulence in mice (*44*) and administration of purified toxin induces numerous effects associated with infection such as histamine sensitization, leukocytosis, and insulin secretion. In terms of protection, it has been difficult to demonstrate a definitive correlation between a humoral response to any antigen and protection against disease, although qualitatively high levels of antibody to PTx are associated with a lower likelihood of developing clinical disease upon exposure to pertussis (*11*, *45*).

After immunization with PTx, antibodies recognizing the S1 subunit are recovered at high frequency (*15*), indicating this subunit as a whole is strongly immunogenic. Analysis of monoclonal antibodies binding PTx has documented the presence of at least four nonoverlapping epitopes on the PTx holotoxin; monoclonal antibodies binding two of these (on the S1 and S2/3 subunits) have been shown to be protective in mouse models (*15*−*17*). Sato et al. performed a detailed comparison of 10 anti-PTx-S1 antibodies, polyclonal anti-PTx sera, and 10 anti-B oligomer antibodies in the mouse aerosol model (*8*). Remarkably, only the 1B7 antibody conferred significant survival when administered between 0 and 7 days after infection while also reducing the number of bacteria and amount of PTx in the lungs (*8*). This anti-PTx-S1 antibody may protect by binding an epitope that prevents substrate access to the catalytic cleft or restricts unfolding of the S1 subunit necessary for translocation to the cytoplasm, while nonprotective anti-PTx-S1 antibodies bind a separate epitope and do not interfere with PTx-S1 function (see Figure 1). The infrequent recovery of antibodies displaying 1B7-like neutralizing activities suggests that (1) the antibody or the epitope recognized possesses unique protective qualities and (2) the epitope is poorly immunogenic.

Location of the Neutralizing Epitope on PTx Recognized by mAb 1B7. Prior efforts to characterize the conformational epitope on PTx-S1 bound by 1B7 using truncations, deletions, and peptide fragments identified two linear subepitopes involved in the binding (amino acids 8−14 and 124−186) (*18*, *21*). These appeared to be independent linear subepitopes as mutations in either region were associated with loss of binding on a Western blot. Since 1B7 inhibits toxin-mediated ADP ribosylation of G proteins in vitro, early reports suggested the antibody may directly and predominately interact with the catalytic residues located in the linear region between amino acids 8 and 14 which shows homology with both cholera toxin and *E. coli* heat labile toxin. The PTx holotoxin structure, published subsequently (*23*), revealed that residues 9−13 are mostly buried (≤13% solvent accessible), making it unlikely that antibodies could interact directly with these in a properly folded protein. However, Western blot analysis showed that 1B7 was unable to bind Y8A and had a weakened ability to bind R13A (see Table 5). The relevance of this linear interaction is unclear since 15-mer PTx-S1 peptides capable of recapitulating this linear binding site could not be identified (*16*). Furthermore, antibody conformational epitope prediction programs, including ElliPro, Discotope, and Pepsurf, did not predict binding residues in this region.

Table 5: Binding Analysis of PTx-S1−220 Variants

PTx	ELISA %$EC_{50\text{-}PTx}$	Western blot mAb 1B7
PTx-S1−220	90 ± 10	+++
9K/129G	60 ± 30	+++
Y8A	< 1	−
R9A	9	+++
Y10A	5	+
D11A	7	+
S12A	20	++
R13A	8	±
E16A	20 ± 10	++
R79A	1 ± 1	±
T81A	30 ± 10	+++
H83A	< 1	+
Y148A	< 1	−
N150A	< 1	±
T153A	11 ± 5	++

Using a combination of experimental and computational techniques, the PTx holotoxin structure, and prior data, we have developed a model of the interaction between PTx and neutralizing antibody 1B7. Using primarily CDR loops L3 and H3, 1B7 binds the base of PTx-S1, possibly engaging in weak interactions with the S4 subunit (see Figure 5). This region of PTx-S1 appears to be readily accessible to antibodies and is fairly flat, consisting of three antiparallel β-sheets and two different turns: one between the aforementioned β-sheets and another prior to an α-helix. The energetically important PTx-S1 residues, assessed by alanine scanning mutagenesis, are R79, H83, N150, and Y148. Chemically, the surface is mostly hydrophobic with one arginine, nine hydrogen bonds, and a solvent-accessible area of ∼1000 $Å^2$, typical for antibody−antigen interactions. Interestingly, both the model and data support a weak stabilizing interaction with the S4 subunit of the B oligomer involving a separate turn between β-sheets. Although only S4 residue A40 was suggested by Pepsurf, because of their proximity, residues S42 and S43 may also be involved in this interaction. Overall, this is a conformational epitope that includes a short linear sequence (Y148−N150 along a β-sheet strand), consistent with 1B7's ability to bind reduced and denatured PTx-S1 on a Western blot. This is consistent with a linear subepitope between amino acids 124 and 186. Binding of mAb 1B7 to the PTx-S1−220 variants, N150A and Y148A, was not detected in the ELISA with up to 1.6 μM antibody.

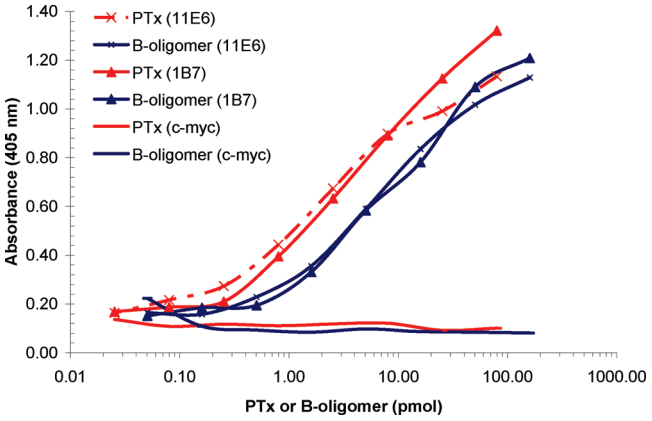

FIGURE 6: ELISA of PTx (red) and the B oligomer (blue) with primary antibody 1B7 (▲), 11E6 (×), or the negative control, c-myc, representing nonspecific antibody binding (no symbol).

Similarly, the 1B7 mAb had a greatly weakened ability to bind N150A and no ability to bind Y148A on a Western blot using very sensitive chemiluminescence detection (see Table 5).

The involvement of the B oligomer in this protective epitope is indicated by the marked reduction in the level of binding of mAb 1B7 to PTx holotoxin [$k_d = (0.4 \pm 0.6) \times 10^3\ s^{-1}$] versus PTx-S1 [$k_d = (1.9 \pm 0.3) \times 10^3\ s^{-1}$]. This reduction in binding affinity is observed with both the commercially prepared S1−235 and the recombinant, truncated S1−220, indicating it is not an artifact of the recombinant version (see Table 1). Interestingly, although both ELISA and SPR analysis measured a weak interaction between the B oligomer and mAb 1B7 (see Figure 6), no recognition of the B oligomer was detected by chemiluminescent Western blotting (see Figure 3). There are three possibilities to explain this result: (1) 1B7 recognizes a separate conformational epitope on the B oligomer at a significantly lower affinity than PTx-S1; (2) 1B7 recognizes a single epitope dominated by PTx-S1 but supplemented by a weak B oligomer interaction; (3) PTx-S1 is stabilized by its interaction with the B oligomer, resulting in reduced entropic costs of 1B7 binding. The model is consistent with the latter two possibilities, but we were unable to directly test these hypotheses due to difficulties in recombinant expression of S4 and reconstitution of holotoxin with PTx-S1 variants. If 1B7 does interact with both the S1 and S4 subunits, this may explain the low frequency at which 1B7-like antibodies are recovered, since the antibody would need to span the A−B subunit interface. Moreover, it suggests a mechanism of protection: 1B7 may act as a molecular staple linking PTx-S1 to the B oligomer, slowing PTx-S1 unfolding and dissociation from the B oligomer in the ER, weakening the ability of PTx-S1 to escape to the cytosol and perform catalysis. Validation of this model by cocrystallization of 1B7 with PTx is ongoing to provide direct experimental evidence of the 1B7 binding site.

Contribution of mAb 1B7 to PTx Recognition. Although previous studies have focused on the 1B7 epitope on PTx-S1, the antibody itself may possess unique qualities that result in effective neutralization. In addition to blocking toxin catalysis, 1B7 binding may, for instance, slow toxin unfolding necessary for escape from the ER into the cytoplasm (see Figure 1). To understand the antibody's role in binding and to aid in the creation of a docked model of the interaction, 12 hu1B7 residues predicted to contribute significantly to the energetics of binding were individually altered to alanine. These experiments identified six key residues required for high-affinity binding to S1: L-F31, L-H94, L-W91, H-S97, H-W33, and H-N58. These six residues are equally distributed over the heavy and light chains, with a slight bias toward CDR L3. Of the CDRs, only L2 contains no key residues and does not appear to contribute significantly to the interaction. This is consistent with most antibody−antigen contacts in which CDR-L2 has the least involvement of all the CDR loops with contacting residues 42% of the time (www.bioinf.org.uk). Of the six key residues, H-W33, L-W91, H-S97, and L-H94 are common interacting residues with contacts in more than 70% of complexes. The other two residues, L-F31 and H-N58, are less common (15 and 38%, respectively). However, mutation of L-F31 to alanine resulted in only weakened binding and is thus not thought to be a large contributor to the interaction. Overall, the residues chosen on 1B7 for analysis using RosettaDock and ZDock were correctly predicted in 50% of the cases. On the basis of these results, further optimization of 1B7 binding could be achieved by targeted mutagenesis of CDRs L3 and H3, which often dominate binding in antibody complexes.

Epitope Conservation across Naturally Occurring and Engineered Strains. A consequence of broad vaccination programs is the potential to select for escape variants of the major virulence factors, which may be accelerated by the use of acellular vaccines. Detailed genotyping of strains, primarily in the Netherlands, has aimed to track naturally occurring and vaccine-induced variation in pertussis antigens (*46*). The naturally occurring mutations in these strains (PTx-S1A, PTx-S1D, and PTx-S1E) are mainly found in the S1 subunit, with each variant containing up to three amino acid substitutions with respect to PTx-S1B (Tohama I) (*47*). The most divergent PTx-S1 gene is found in *B. bronchiseptica*, with four amino acid mutations, but is not expressed due to promoter mutations (*39*, *46*).

Given this modest level of natural variation, a key question is whether variation impacts the 1B7 epitope and, if so, whether 1B7 binds these variants with the same affinity. After expression and purification of truncated versions (residues 1−220) of three of the four naturally occurring strain variants, we found that PTx-S1E is bound by 1B7 with identical (within error) off rates versus WT PTx-S1−220 (see Table 1). However, 1B7 exhibited an ~2-fold decrease in off rates with respect to PTx-S1A and PTx-S1D, indicating an increase in affinity. A second question is whether the catalytically inactive PTx-S1 variant used in some acellular vaccines (containing amino acid substitutions R9K and E129G) will also be recognized by 1B7. 1B7 binds this PTx-S1 variant with an affinity identical to that of WT (within error), suggesting that acellular vaccines containing the R9K/E129G variant will be able to elicit 1B7-like protective antibodies. The value of the 1B7 epitope as a target for passive immunization and a potential correlate of protective immunity will depend both on its ability to elicit neutralizing 1B7-like antibodies and on conservation within the pool of circulating clinical strains. The ability of hu1B7 to bind existing PTx-S1 variants indicates that the epitope recognized by 1B7 is conserved in the presence of natural antigenic drift.

Mechanism of PTx Neutralization by mAb 1B7. When originally characterized, mAb 1B7 was thought to protect against toxin effects by blocking catalysis, either by directly associating with catalytic residues or blocking substrate access to these residues. However, several other monoclonal antibodies that block ADP ribosylation in vitro but are not neutralizing in vivo have been characterized (*15*). Furthermore, the mechanism of toxin cellular binding and internalization has been characterized

in detail, and it is not clear whether an antibody would remain associated with PTx-S1 during retrograde transport: at the low pH of the endosome, the reducing environment of the ER, or during translocation into the cytoplasm (see Figure 1). The fact that 1B7 can bind reduced and unfolded PTx-S1 on a Western blot and under the cytoplasmic conditions replicated during in vitro ADP ribosylation assays suggests that it could block catalysis in the cytoplasm if present in that compartment, but 1B7 ligation may protect by altering PTx trafficking within the cell.

Burns and colleagues (*39*) demonstrated that PTx is transiently expressed on the bacterial cell surface during secretion, and *B. pertussis* knockout mutants have shown that along with FHA, PTx is necessary and sufficient for bacterial adherence. Thus, 1B7 may bind whole bacteria, blocking the adhesion of bacteria to respiratory epithelial cells or potentially mediating effector functions. 1B7 was isolated as a murine IgG2a antibody, an isotype able to opsonize bacteria and fix complement, while murine IgG1 isotypes are more commonly associated with toxin neutralization or blocking bacterial adherence. It is not clear if the isotype has mechanistic relevance or is a result of the Th1/Th2 bias induced by the toxin itself. $F(ab')_2$ fragments of anti-PTx antibodies (*48*) and Fab fragments of 1B7 (*15*) displayed identical in vitro CHO clustering effects as the parental monoclonal antibody. While the requirement for an Fc has not been directly tested in vivo, anti-PTx antibodies in human immune sera do not display opsonic activity or induce phagocytosis by human leukocytes (*7*, *11*). Similar to other toxin-mediated diseases, such as botulinum and anthrax (*49*), toxin neutralization may not require Fc-mediated effector functions but remains an intriguing area of future investigation.

CONCLUSIONS

We have identified a uniquely neutralizing epitope on PTx using PTx-S1 variants and humanized scAb versions of the 1B7 monoclonal antibody. This epitope is adjacent to but does not include the catalytically active residues on PTx-S1 and spans the junction between the S1 and S4 subunits. This model suggests a mechanism of 1B7 antibody protection: antibody ligation may anchor the catalytically active S1 subunit to the B oligomer, thereby preventing PTx-S1 dissociation and subsequent transport into the cytosol, where PTx-S1 disrupts G-protein signaling. Confirmation of this model awaits additional cocrystallization and cellular experiments of antibody−toxin complex trafficking within cell. Notably, numerous anti-PTx-S1 antibodies have been produced with the ability to neutralize in vitro ADP ribosylation activity, but most perform poorly in in vivo mouse models of disease. Thus, we propose that the molecular details of epitope recognition are critical in discriminating between antibodies capable of in vitro and in vivo protection and that this epitope is a unique target to exploit for passive immunotherapy and acellular vaccine design. Moreover, it suggests that the search for immune correlates in pertussis may require careful examination of serum responses to specific epitopes, not just individual virulence factors (*20*, *22*).

ACKNOWLEDGMENT

We gratefully acknowledge transfer of the 1B7 and 11E6 hybridomas from Jerry Keith (National Institutes of Health, Bethesda, MD).

REFERENCES

1. Kerr, J. R. (2000) Pathogenesis of human parvovirus B19 in rheumatic disease. *Ann. Rheum. Dis. 59*, 672–683.
2. Roush, S. W., and Murphy, T. V. (2007) Historical comparisons of morbidity and mortality for vaccine-preventable diseases in the United States. *JAMA 298*, 2155–2163.
3. Jadhav, S. S., and Gairola, S. (1999) Composition of acellular pertussis and combination vaccines: A general review. *Biologicals 27*, 105–110.
4. Kamachi, K., Konda, T., and Arakawa, Y. (2003) DNA vaccine encoding pertussis toxin S1 subunit induces protection against *Bordetella pertussis* in mice. *Vaccine 21*, 4609–4615.
5. Pichichero, M. E.; et al. (2006) Acellular pertussis vaccine booster combined with diphtheria and tetanus toxoids for adolescents. *Pediatrics 117*, 1084–1093.
6. Taranger, J.; et al. (2000) Correlation between pertussis toxin IgG antibodies in postvaccination sera and subsequent protection against pertussis. *J. Infect. Dis. 181*, 1010–1013.
7. Hellwig, S. M.; et al. (2003) Crucial role of antibodies to pertactin in *Bordetella pertussis* immunity. *J. Infect. Dis. 188*, 738–742.
8. Sato, H., and Sato, Y. (1990) Protective activities in mice of monoclonal antibodies against pertussis toxin. *Infect. Immun. 58*, 3369–3374.
9. Bruss, J. B., and Siber, G. R. (1999) Protective effects of pertussis immunoglobulin (P-IGIV) in the aerosol challenge model. *Clin. Diagn. Lab. Immunol. 6*, 464–470.
10. Bruss, J. B., and Siber, G. R. (2002) Quantitative priming with inactivated pertussis toxoid vaccine in the aerosol challenge model. *Infect. Immun. 70*, 4600–4608.
11. Cherry, J. D.; et al. (1998) A search for serologic correlates of immunity to *Bordetella pertussis* cough illnesses. *Vaccine 16*, 1901–1906.
12. Halperin, S. A.; et al. (2007) Is pertussis immune globulin efficacious for the treatment of hospitalized infants with pertussis? No answer yet. *Pediatr. Infect. Dis. J. 26*, 79–81.
13. Weingart, C. L.; et al. (2000) Characterization of bactericidal immune responses following vaccination with acellular pertussis vaccines in adults. *Infect. Immun. 68*, 7175–7179.
14. Mills, K. H. (2001) Immunity to *Bordetella pertussis*. *Microbes Infect. 3*, 655–677.
15. Sato, H., Sato, Y., and Ohishi, I. (1991) Comparison of pertussis toxin (PT)-neutralizing activities and mouse-protective activities of anti-PT mouse monoclonal antibodies. *Infect. Immun. 59*, 3832–3835.
16. Kim, K. J.; et al. (1989) Epitopes on the S1 subunit of pertussis toxin recognized by monoclonal antibodies. *Infect. Immun. 57*, 944–950.
17. Kenimer, J. G.; et al. (1989) Monoclonal antibodies to pertussis toxin: Utilization as probes of toxin function. *Hybridoma 8*, 37–51.
18. Bartoloni, A.; et al. (1988) Mapping of a protective epitope of pertussis toxin by *in vitro* refolding of recombinant fragments. *Nat. Biotechnol. 6*, 709–712.
19. Cieplak, W.; et al. (1988) Identification of a region in the S1 subunit of pertussis toxin that is required for enzymatic activity and that contributes to the formation of a neutralizing antigenic determinant. *Proc. Natl. Acad. Sci. U.S.A. 85*, 4667–4671.
20. Raupach, B., and Schmidt, M. A. (1994) Elucidation of linear epitopes of pertussis toxin using overlapping synthetic decapeptides: Identification of a human B-cell determinant in the S1 subunit indicative of acute infections. *Microb. Pathog. 17*, 213–226.
21. Burnette, W. N.; et al. (1988) Pertussis toxin S1 mutant with reduced enzyme activity and a conserved protective epitope. *Science 242*, 72–74.
22. Kaslow, H. R.; et al. (1992) Detection of antibodies inhibiting the ADP-ribosyltransferase activity of pertussis toxin in human serum. *J. Clin. Microbiol. 30*, 1380–1387.
23. Stein, P. E.; et al. (1994) The crystal structure of pertussis toxin. *Structure 2*, 45–57.
24. Krueger, K. M., and Barbieri, J. T. (1994) Assignment of functional domains involved in ADP-ribosylation and B-oligomer binding within the carboxyl terminus of the S1 subunit of pertussis toxin. *Infect. Immun. 62*, 2071–2078.
25. Krebber, A.; et al. (1997) Reliable cloning of functional antibody variable domains from hybridomas and spleen cell repertoires employing a reengineered phage display system. *J. Immunol. Methods 201*, 35–55.
26. Hayhurst, A.; et al. (2003) Isolation and expression of recombinant antibody fragments to the biological warfare pathogen Brucella melitensis. *J. Immunol. Methods 276*, 185–196.
27. Hemsley, A.; et al. (1989) A simple method for site-directed mutagenesis using the polymerase chain reaction. *Nucleic Acids Res. 17*, 6545–6551.

28. Hayhurst, A., and Harris, W. J. (1999) *Escherichia coli* skp chaperone coexpression improves solubility and phage display of single-chain antibody fragments. *Protein Expression Purif. 15*, 336–343.
29. Hewlett, E. L.; et al. (1983) Induction of a novel morphological response in Chinese hamster ovary cells by pertussis toxin. *Infect. Immun. 40*, 1198–1203.
30. Whitelegg, N. R., and Rees, A. R. (2000) WAM: An improved algorithm for modelling antibodies on the WEB. *Protein Eng. 13*, 819–824.
31. Sood, V. D., and Baker, D. (2006) Recapitulation and design of protein binding peptide structures and sequences. *J. Mol. Biol. 357*, 917–927.
32. Chen, R., and Weng, Z. (2002) Docking unbound proteins using shape complementarity, desolvation, and electrostatics. *Proteins 47*, 281–294.
33. Lyskov, S., and Gray, J. J. (2008) The RosettaDock server for local protein-protein docking. *Nucleic Acids Res. 36*, W233–W238.
34. Kortemme, T., and Baker, D. (2002) A simple physical model for binding energy hot spots in protein-protein complexes. *Proc. Natl. Acad. Sci. U.S.A. 99*, 14116–14121.
35. Kortemme, T., Kim, D. E., and Baker, D. (2004) Computational alanine scanning of protein-protein interfaces. *Sci. STKE 2004*, pl2.
36. Mayrose, I.; et al. (2007) Epitope mapping using combinatorial phage-display libraries: A graph-based algorithm. *Nucleic Acids Res. 35*, 69–78.
37. Felici, F.; et al. (1993) Mimicking of discontinuous epitopes by phage-displayed peptides, II. Selection of clones recognized by a protective monoclonal antibody against the *Bordetella pertussis* toxin from phage peptide libraries. *Gene 128*, 21–27.
38. Pizza, M.; et al. (1989) Mutants of pertussis toxin suitable for vaccine development. *Science 246*, 497–500.
39. Hausman, S. Z., and Burns, D. L. (2000) Use of pertussis toxin encoded by ptx genes from *Bordetella bronchiseptica* to model the effects of antigenic drift of pertussis toxin on antibody neutralization. *Infect. Immun. 68*, 3763–3767.
40. Braden, B. C.; et al. (1995) Structure and thermodynamics of antigen recognition by antibodies. *Ann. N.Y. Acad. Sci. 764*, 315–327.
41. Davies, D. R., and Cohen, G. H. (1996) Interactions of protein antigens with antibodies. *Proc. Natl. Acad. Sci. U.S.A. 93*, 7–12.
42. Viswanathan, M.; et al. (1996) Modeling the structure of the combining site of an antisweet taste ligand monoclonal antibody NC10.14. *Biopolymers 39*, 395–406.
43. Yang, J.; et al. (2003) Dissecting cooperative and additive binding energetics in the affinity maturation pathway of a protein-protein interface. *J. Biol. Chem. 278*, 50412–50421.
44. Weiss, A. A.; et al. (1983) Tn5-induced mutations affecting virulence factors of *Bordetella pertussis*. *Infect. Immun. 42*, 33–41.
45. Storsaeter, J.; et al. (1998) Levels of anti-pertussis antibodies related to protection after household exposure to *Bordetella pertussis*. *Vaccine 16*, 1907–1916.
46. Mooi, F. R., van Loo, I. H., and King, A. J. (2001) Adaptation of *Bordetella pertussis* to vaccination: A cause for its reemergence? *Emerging Infect. Dis. 7*, 526–528.
47. Makinen, J.; et al. (2002) Rapid typing of *Bordetella pertussis* pertussis toxin gene variants by LightCycler real-time PCR and fluorescence resonance energy transfer hybridization probe melting curve analysis. *J. Clin. Microbiol. 40*, 2213–2216.
48. Sato, H.; et al. (1987) Effect of monoclonal antibody to pertussis toxin on toxin activity. *Infect. Immun. 55*, 909–915.
49. Maynard, J. A.; et al. (2002) Protection against anthrax toxin by recombinant antibody fragments correlates with antigen affinity. *Nat. Biotechnol. 20*, 597–601.
50. Hazes, B.; et al. (1996) Crystal structure of the pertussis toxin-ATP complex: A molecular sensor. *J. Mol. Biol. 258*, 661–671.